Supplementary Information for

Controls on Iron Reduction and Biomineralization over Broad Environmental Conditions as Suggested by the Firmicutes *Orenia metallireducens* Strain Z6

Yiran Dong[1,2]*, Robert A. Sanford[3], Maxim I. Boyanov[4,5], Theodore M. Flynn[4†], Edward J. O'Loughlin[4], Kenneth M. Kemner[4], Samantha George[6], Kaitlyn E. Fouke[7], Shuyi Li[1], Dongmei Huang[1], Shuzhen Li[1], Bruce W. Fouke[2,3,6]

School of Environmental Studies, China University of Geosciences (Wuhan)[1]

Carl R. Woese Institute for Genomic Biology, University of Illinois Urbana-Champaign[2]

Department of Geology, University of Illinois Urbana-Champaign[3]

Biosciences Division, Argonne National Laboratory[4]

Institute of Chemical Engineering, Bulgarian Academy of Sciences, Bulgaria[5]

Department of Microbiology, University of Illinois Urbana-Champaign[6]

Marine Biological Laboratory, Woods Hole[7]

*Corresponding author. Mailing address: 388 Lumo Road, Wuhan, China. Phone: +86-27-67883152. Email: dongyr@eug.edu.cn

[†]Current address: California Department of Water Resources, West Sacramento, CA

Number of pages: 37; **Number of figures**: 19; **Number of tables**: 4.

Materials and Methods

Synthesis of different iron minerals. Ferrihydrite [Fe_2O_3•0.5H_2O], hematite (α-Fe_2O_3), lepidocrocite [γ-FeO(OH)], goethite [α-FeO(OH)] and magnetite (Fe_3O_4) were prepared as described[4]. Ferrihydrite was prepared by titrating 0.5 M $FeCl_3$ to pH 7.5 by the dropwise addition of 1.0 M KOH with continuous mixing. Goethite was synthesized by aging ferrihydrite under alkaline conditions at 70 °C for 60 h. Hematite was synthesized by the forced hydrolysis of a 0.02 M solution of $FeCl_3$ in 0.002 M HCl at 98 °C for 10 d. Lepidocrocite was synthesized by air oxidation of a ferrous chloride solution. Briefly, 30 g of $FeCl_2$•4H_2O was dissolved in 900 mL of water and the resulting solution was filtered through a 0.2 μm nylon filter to remove any Fe(III) solids present. The pH of the solution was adjusted to 6.0 with 0.5 M NaOH and the resulting blue/green suspension was sparged with air. The pH of the suspension was maintained at pH 5.5-6.0 by the dropwise addition of 0.5 M NaOH until base consumption ceased (~1 h). The synthesis was conducted in a large > 4 L capacity desiccator. Subsequent to synthesis, all phases were repeatedly washed by centrifugation and re-suspension in Milli-Q® H_2O (18.2 MΩ•cm), then dried at 60 °C and ground to pass a 200 mesh sieve (ferrihydrite was washed, but not dried). Magnetite (Fe_3O_4) was prepared by dissolving 8.0 g of $FeSO_4$•7H_2O in 560 mL of anoxic distilled water. The resulting solution was transferred to a 1.5 L 90 ºC water-jacketed reaction flask with continuous purging with Ar. Once the Fe(II) solution reached 90 ºC, 240 mL of an anoxic solution containing 6.46 g of KNO_3 and 44.9 g of KOH was added dropwise over 5 min, after which the resulting black suspension was kept mixed and maintained at 90 ºC for 1 h. After cooling to ambient temperature, the suspension was transferred to an anoxic glovebox and washed repeatedly with anoxic distilled water and maintained as an aqueous suspension. The crystal structure of the synthesized minerals was confirmed using a Siemens/Bruker D-5000 X-

ray Diffractometer (XRD) (Siemens, Germany) and the morphology was observed using a JOEL 6060LV General Purpose SEM as described below (Fig. S17).

Sample collection and chemical analyses. At intervals of 1-5 days, 0.2 mL of the well-mixed culture was collected using a sterile 1-mL syringe (Becton, Dickinson and Company, NJ), which was promptly acidified by addition of 0.2 mL of 1 M HCl and incubated for 1 hour for determination of total iron and acid-extractable Fe(II). The acid extraction time (1 hour) was selected based on two major criteria: 1) the majority of secondary minerals could be extracted within this period[5], which was verified in our preliminary experiment; and 2) magnetite was not extracted to avoid overestimation of iron reduction in the samples with this mineral as the substrate (Condition 17 in Table S1). To quantify the dissolved Fe(II) [Fe(II)(aq)], an additional 0.2 mL of culture suspension was collected inside an anoxic chamber filled with N_2:H_2 (95:5, v:v) (Coy Laboratory Products, MI), and centrifuged at 4,000 × g for 3 min, after which the supernatant was removed and acidified with 0.2 mL of 1 M HCl.

The concentrations of ferrous iron and total iron were measured using the ferrozine method[6, 7] and analyzed with a Genesys 20 spectrophotometer (Thermo Fisher Scientific Inc., MA) at 562 nm as described by Lovley and Phillips[8]. When measuring total iron concentrations, an additional 400 μL of 2.5 M HCl was added into the pre-acidified samples which were then heated at 50°C to dissolve all the ferric iron oxides. Then, Fe(III) was reduced to Fe(II) using hydroxylamine hydrochloride before the total Fe(II) was measured using the ferrozine method[9]. Fe(III) concentrations were calculated by subtracting the concentrations of ferrous iron from total iron. At the end of the experiments, the solid-associated Fe(II) [Fe(II)(s)] was calculated as the difference between acid extractable Fe(II) and Fe(II) (aq).

71 The saturation index for the potential secondary minerals was calculated using
72 Geochemist's Workbench (Aqueous Solutions LLC) based on the components of the media, the
73 incubation conditions, and the measured total acid-extractable Fe(II).
74
75 **Mineral characterization by imaging and spectroscopic methods.** Scanning electron
76 microscopy with energy dispersive X-ray spectroscopy (SEM-EDX), X-ray diffraction (XRD),
77 Fe-edge X-ray absorption near edge structure (XANES) spectroscopy, and X-ray absorption fine
78 structure (EXAFS) spectroscopy[11] were applied to determine the morphology and composition of
79 the secondary minerals. The samples for SEM-EDX imaging were prepared as described by
80 O'Loughlin et al.[10] Specimens were transferred into 50 mL conical tubes inside the anoxic
81 chamber and were kept inside the tubes during transport to the laboratory for SEM analyses. The
82 samples were briefly (< 30 s) exposed to air during transfer to the JOEL 6060LV General
83 Purpose SEM.
84 The XRD analysis of secondary mineralization products employed a Siemens/Bruker D-
85 5000 X-ray diffractometer with Ni-filtered Cu K_α radiation (Bruker Cooperation, Germany).
86 Samples for XRD analysis were collected inside the anoxic chamber by filtration through 25-mm
87 diameter, 0.22-µm nylon filters, which were promptly covered with Kapton® film under anoxic
88 conditions[10]. Samples prepared in this manner showed no evidence of oxidation during analysis.
89 The scan was conducted typically between 10 and 80 2θ at a speed of 1 2θ min^{-1}. For some
90 samples (e.g., Lep-pH 8.5), 5 to 80 2θ was scanned at the same speed. The XRD profiles were
91 analyzed with the JADE 7 software package (MDI, Livermore, CA). Elemental analysis was
92 conducted using a Quantax 80 EDS system (Bruker Nano GmbH, Germany).

93 Fe K-edge (7, 112 eV) X-ray absorption spectroscopy measurements were carried
94 out at the MR-CAT/EnviroCAT bending magnet beamline (Sector 10, Advanced Photon
95 Source)[12]. XANES and EXAFS spectra were collected from the standards and the reactor
96 solids in transmission mode using gas-filled ionization detectors. The reactor solids were
97 separated by filtration through a 0.22 μm PTFE filter inside the anaerobic chamber and
98 the hydrated filter cake was sealed together with the separation membrane between
99 two layers of Kapton film. Spectra were collected at room temperature inside a N_2-
100 purged sample cell. Anoxic integrity of samples prepared and analyzed this way have
101 been demonstrated in previous work[13]. Energy calibration was established by setting the
102 inflection point in the spectrum from an Fe foil to 7,112 eV and maintained continuously
103 afterwards by collecting data from the foil simultaneously with the collection of data
104 from the samples. Radiation-induced changes in the spectra were not observed. No
105 differences were observed between spectra from different areas on the sample so all
106 scans from each sample were averaged to produce the final spectrum.
107 Analyses of the spectra involved comparisons to Fe-containing standards
108 followed by combinatorial linear combination (LC) fitting to extract the spectral weight
109 of up to three standards that best describe the experimental spectra of the bioreactors.
110 Combinatorial LC fitting involves refining the experimental data with all combinations of
111 the standards spectra (fit components) and ranking the fits according to a goodness-of-
112 fit indicator (chi-squared). Fits were done with all distinct combinations of 2 and 3

components. When the improvement in the fit with a third component was not deemed significant (i.e., the chi-squared was not decreased by more than 30% relative to the best fit with two components), the fit with only two components was chosen as the best fit to the data. The standards dataset used here included the parent iron oxides and potential biotransformation products: ferrihydrite, lepidocrocite, goethite, hematite, magnetite, phosphate-stabilized carbonate green rust, freshly-precipitated and annealed siderite (referred to as amorphous siderite and crystalline siderite), vivianite, dissolved Fe(II) (Fe2aq), Fe(II) adsorbed to carboxyl resin (Fe2ads), $Fe(OH)_2$, synthetic ferrous hydroxy-carbonate (chukanovite), mackinawite, and ferrous oxide. The Fe-containing standards were measured and characterized in this and in previous work at the same beamline[14-19]. The polycrystalline powder standards were mounted on the adhesive side of Kapton tape and their absorption spectra were measured in transmission. Solution samples were mounted in a 1.5 mm thick sample holder with Kapton film windows and the spectrum was measured in fluorescence. Adsorbed Fe standards were mounted as wet pastes in a 1.5 mm thick sample holder with Kapton windows and measured in fluorescence mode. Normalization and background removal of the data was done using the program AUTOBK[20]. The combinatorial LC fits were performed using the program ATHENA[21]. Only the secondary minerals with relative abundance higher than 10 % were included in the mineralogical analyses by EXAFS.

We observed a limitation in differentiating freshly-precipitated siderite from adsorbed Fe(II) or from vivianite at low relative amounts (e.g. <15-20% of total Fe) in the LC fits. Figure

S18 shows an overlay of the EXAFS spectra from Fe(II) adsorbed to carboxyl surface groups, amorphous siderite, and vivianite. It can be seen that the phase and amplitudes of the EXAFS signals are similar between these pure Fe(II) phases, and that the spectral differences are in the finer features resulting from the different binding environments and corresponding outer shell molecular structure. While the outer-shell spectral differences can be used for identification of the pure phases, the selectivity between these three phases decreases significantly at lower relative contents, particularly when more than one of them is present in the sample. Because the EXAFS analysis showed that most of the bioreduced reactors contained significant amounts of amorphous siderite, our ability to detect and quantify <15% of total Fe as vivianite in these particular systems is uncertain. Although vivianite is detected in the XRD patterns, we could not unequivocally confirm or quantify its presence together with the larger siderite component. We have therefore chosen to quantify only the larger siderite spectral component, with the understanding that up to about 10% of the siderite component may in some cases be due to the presence of vivianite.

Assessment of Fe(II) analyzed by acid extraction versus by XANES. In most cases, Fe(II)(s) determined by the extraction and the XANES techniques were within the measurement uncertainty. However, several of the samples in Table 1 show differences in the amount of Fe(II)(s) determined by the two techniques. We can attribute the differences to the different times that the samples for the two techniques were taken and/or to the different approaches used for collecting and separating the solids.

Specifically, there was a one week gap between the 0.5N HCl extraction and the sampling for XANES analysis. It is possible that the additional incubation resulted in further

mineral diagenesis for some sample sets during that time. For separation of solids, samples were taken through a septum in the bottle and centrifuged for the 0.5N HCl extraction analysis. Since ferrous minerals are known to stick to the bottle surface, the total Fe(II) + Fe(III) was lower than the initial mass of Fe(III) added. Since the percentages shown in Table 1 used the initial ferric mineral concentration as the total iron, the depleted Fe(II) in the acid extract leads to an artificially low percentage of Fe(II) solids. For XANES analysis, reactor bottles were opened and the entire contents filtered to collect the solids. In addition to this filtration occurring a week after the acid extraction, it is possible in a couple of cases that ferrous iron particles (<0.2 μm) may have passed through the filter and been missed during the XANES analysis. This would lead to lower percentages of Fe(II) minerals in XANES analysis and we note this only occurred twice.

To ensure that the sampling and measurement uncertainties in either method did not bias our conclusions, we re-plotted some of the figures in our study using the two sets of Fe(II) analyses. As illustrated in Fig. S19, the Fe(II)/Fe(III) determined by either method could not explain the formation of the observed biominerals. Therefore, the inconsistency in the Fe(II)(s) percentages obtained by the different methods does not affect the overall conclusion of this study.

Saturation Indices and Phase Characterization. Calculated saturation indices of potential biogenic minerals indicated that the incubation solutions were oversaturated with respect to vivianite (in the presence of phosphate), siderite, and magnetite by 6.9-12.3, 1.9-5.2 and 1.3-11.4 orders of magnitude, respectively (Table S2). GR-CO_3 formation was favored under most conditions except for the ones amended with crystalline hematite, goethite, or magnetite, in which significantly less iron reduction occurred, or when the pH was low (Lep-pH 6.5). In

addition to these Fe(II)-containing biogenic minerals, the formation of secondary Fe(III) minerals (e.g., hematite and goethite) was favorable in all the cultures amended with ferrihydrite or lepidocrocite. However, production of hematite as the secondary mineral was detected only under a few conditions in the ferrihydrite-reducing cultures (Tables 1 and S1). In comparison, although positive saturation index values were observed for magnetite under all the culturing conditions, it was only observed as a minor secondary mineral in cultures amended with lepidocrocite at elevated pH (Lep-pH 8.5) (Tables 1 and S2).

Table S1. Experimental conditions designed to test the effects of different geochemical factors on biomineralization by strain Z6.

IDs	Factor	Ferric iron substrate (mM)[a]	Temp. (°C)	Salinity (g/L NaCl)	pH	Buffer (mM)	Headspace (v:v)	Phosphate (mM)	Sulfate (mM)[b]	AQDS (μM)[b]
1	T	lepidocrocite (20)	22	20	7.2	bicarbonate (25)	N_2:CO_2 (90:10)	2.5	-	-
2		lepidocrocite (20)	50	20	7.2	bicarbonate (25)	N_2:CO_2 (90:10)	2.5	-	-
3	Salinity	lepidocrocite (20)	37	35	7.2	bicarbonate (25)	N_2:CO_2 (90:10)	2.5	-	-
4		lepidocrocite (20)	37	50	7.2	bicarbonate (25)	N_2:CO_2 (90:10)	2.5	-	-
5		lepidocrocite (20)	37	100	7.2	bicarbonate (25)	N_2:CO_2 (90:10)	2.5	-	-
6		lepidocrocite (20)	37	150	7.2	bicarbonate (25)	N_2:CO_2 (90:10)	2.5	-	-
7	pH	lepidocrocite (20)	37	20	6.5	bicarbonate (25), PIPES (10)	N_2:CO_2 (90:10)	2.5	-	-
8		lepidocrocite (20)	37	20	8.5	TAPS (25)[c]	N_2 (100)	2.5	-	-
9	Anions	lepidocrocite (20)	37	20	7.2	bicarbonate (25)	N_2:CO_2 (90:10)	0	-	-
10		lepidocrocite (20)	37	20	7.2	bicarbonate (25)	N_2:CO_2 (90:10)	6	-	-
11		lepidocrocite (20)	37	20	7.2	bicarbonate (25)	N_2:CO_2 (90:10)	2.5	20	-
12	Electron shuttle	lepidocrocite (20)	37	20	7.2	bicarbonate (25)	N_2:CO_2 (90:10)	2.5	-	100
13	Ferric minerals	ferrihydrite (20)	37	20	7.2	bicarbonate (25)	N_2:CO_2 (90:10)	2.5	-	-
14[d]		**lepidocrocite (20)**	**37**	**20**	**7.2**	**bicarbonate (25)**	**N_2:CO_2 (90:10)**	**2.5**	**-**	**-**
15		hematite (10)	37	20	7.2	bicarbonate (25)	N_2:CO_2 (90:10)	2.5	-	-
16		goethite (20)	37	20	7.2	bicarbonate (25)	N_2:CO_2 (90:10)	2.5	-	-
17		magnetite (6.3)	37	20	7.2	bicarbonate (25)	N_2:CO_2 (90:10)	2.5	-	-

[a.] Different amounts of the corresponding minerals were added for the nominal initial concentration of Fe(III) ~20 mM; [b.] No substrates was amended if not mentioned; [c.] TAPS was used to replace bicarbonate under the alkaline condition to avoid precipitation of calcium carbonate; [d.] This condition was used as the internal reference in the investigation of impacts of multiple geochemical factors on biomineralization during iron reduction as one of the parameters was changed under the other conditions.

Table S2. Calculated saturation index values using GWB for the secondary minerals under different culturing conditions

Conditions[a]	Saturation Index[b]						
	Vivanite	**Siderite**	**Magnetite**	**GR-CO_3**	**Fe$(OH)_2$**	**Hematite**	**Goethite**
Temperature							
Lep-22 °C	9.0	2.5	3.5	1.4	-1.6	2.5	0.8
Lep-37 °C[b]	9.7	2.9	5.4	3.9	-0.6	3.5	1.2
Lep-50 °C	9.7	3.2	6.7	5.1	-0.1	4.2	1.6
Salinity							
Lep-2% NaCl[b]	9.7	2.9	5.4	3.9	-0.6	3.5	1.2
Lep-3.5% NaCl	9.1	2.8	5.2	3.2	-0.8	3.5	1.2
Lep-5% NaCl	8.3	2.6	5.1	2.5	-1.0	3.5	1.2
Lep-10% NaCl	7.7	2.4	5.0	2.0	-1.1	3.5	1.2
Lep-15% NaCl	6.9	2.2	4.8	1.1	-1.3	3.5	1.2
pH							
Lep-pH 6.5	8.2	2.2	4.1	-0.8	-2.0	3.5	1.2
Lep-pH 7.2[b]	9.7	2.9	5.4	3.9	-0.6	3.5	1.2
Lep-pH 8.5	12.3	NA	8.2	NA	2.2	3.5	1.2
Anions and electron shuttle							
Lep-No HPO_4^{2-}	NA[c]	2.9	5.4	3.8	-0.6	3.5	1.2
Lep-HPO_4^{2-} (2.5 mM)[b]	9.7	2.9	5.4	3.9	-0.6	3.5	1.2
Lep-HPO_4^{2-} (6 mM)	10.8	3.1	5.6	NA	-0.5	3.5	1.2
Lep-SO_4^{2-} (20 mM)	9.5	3.0	5.4	4.0	-0.62	3.5	1.2
Lep-AQDS (100 mM)	10.1	3.2	5.6	5.0	-0.37	3.5	1.2
Minerals							
Ferrihydrite	9.5	2.9	11.4	9.6	-0.7	9.6	4.3
Lepidocrocite[b]	9.7	2.9	5.4	3.9	-0.6	3.5	1.2
Hematite	8.0	2.3	1.3	-2.2	-1.3	NA	-0.5
Goethite	7.1	2.0	2.0	-2.3	-1.6	1.0	NA
Magnitite	7.2	1.9	NA	-5.3	-2.2	NA	-0.5

[a.] "Lep" indicates lepidocrocite;
[b.] The cultures prepared with 20 mM lepidocrocite, 2% NaCl, at pH 7.2, with 2.5 mM phosphate, no sulfate and AQDS, and at temperature 37 °C were used as the internal reference set;
[c.] NA: not produced or not available.

Table S3. Linear combination fits of the XANES and EXAFS data

Conditions	LC fit component, EXAFS (% of total Fe)[a]					XANES
	Siderite[b]	Green rust	Hematite	Other altered ferric minerals	Remaining parent substrate	Fe(III)/ Total Fe(s)[c]
Temperature						
Lep-22 °C	36				64	58
Lep-37 °C[d]	**25**	**12**			**63**	**70**
Lep-50 °C	55	11			34	33
Salinity						
Lep-2% NaCl[d]	**25**	**12**			**63**	**70**
Lep-3.5% NaCl	41				59	56
Lep-5% NaCl	16				84	87
Lep-10% NaCl	38				62	60
Lep-15% NaCl	22				78	71
pH						
Lep-pH 6.5	88[e]				12	0
Lep-pH 7.2[d]	**25**	**12**			**63**	**70**
Lep-pH 8.5	29	71				22
Anions and electron shuttle						
Lep-No HPO_4^{2-}	70			11[f]	19	31
Lep-2.5 mM HPO_4^{2-}[d]	**25**	**12**			**63**	**70**
Lep-HPO_4^{2-} (6 mM)	73	14			13	0
Lep-SO_4^{2-} (20 mM)	41	38			21	33
Lep-AQDS (100 mM)	62	38				15
Minerals						
Ferrihydrite (abiotic control)	13		32		55	86
Ferrihydrite	35		44		21	59
Lepidocrocite[d]	**25**	**12**			**63**	**70**

Hematite	18			82	88
Goethite	7			93	88
Magnetite			10[g]	90	68

[a.] The uncertainty in our specific systems is within the generally accepted 10% in LC EXAFS analyses. Here, a 3-component fit is presented if the components' content is higher than 10 % and if it was a statistical improvement over the 2-conponent fits. Otherwise, the best fit with only 2-components is presented. More information on the fitting approach can be found in the Methods and Material section above;

[b.] If not mentioned specifically, amorphous siderite provided a better fit to the data; up to 10% of the Fe(II) component listed here as siderite could be vivianite, adsorbed Fe(II), or FHC; see text under "Mineral characterization by imaging and spectroscopic methods" for clarification;

[c.] This column lists Fe(III) as percentage of total Fe in the solids (balance is Fe(II)), so it can be compared to the extraction data;

[d.] The experimental conditions shown in bold are for the same sample (No. 14 in Table S1), which is listed repeatedly here for easier comparison within each parameter series;

[e.] Siderite identified under this condition contained both crystalline and amorphous siderite with the relative abundance 68% and 20%, respectively;

[f.] LC EXAFS analysis could not differentiate between a ferrihydrite and a goethite component at an 11% content;

[g.] The LC EXAFS fits could not differentiate statistically between hematite, goethite, and ferrihydrite at 10% content.

Table S4. Calculation of aqueous phosphate complexes in the media modeled using GWB

	2.5 mM Phosphate	**6 mM Phosphate**
$NaHPO_4^-$ (mM)	0.81	1.66
$FeHPO_4$ (mM)	0.74	2.14
HPO_4^{2-} (mM)	0.45	0.92
$MgHPO_4$ (mM)	0.17	0.33
$FeH_2PO_4^+$ (mM)	0.13	0.39
$H_2PO_4^-$ (mM)	0.12	0.25
$CaHPO_4$ (mM)	0.10	0.20
$FePO_4^-$ (mM)	6.32E-02	0.18
$KHPO_4^-$ (mM)	2.30E-02	4.64E-02
$MgH_2PO_4^+$ (mM)	9.41E-03	1.86E-02
$MgPO_4^-$ (mM)	7.85E-03	1.55E-02
$CaPO_4^-$ (mM)	6.99E-03	1.40E-02
H_3PO_4 (mM)	8.46E-07	1.71E-06
Fe-phosphate complexes	0.93	2.71
Total phosphate	2.64	6.16

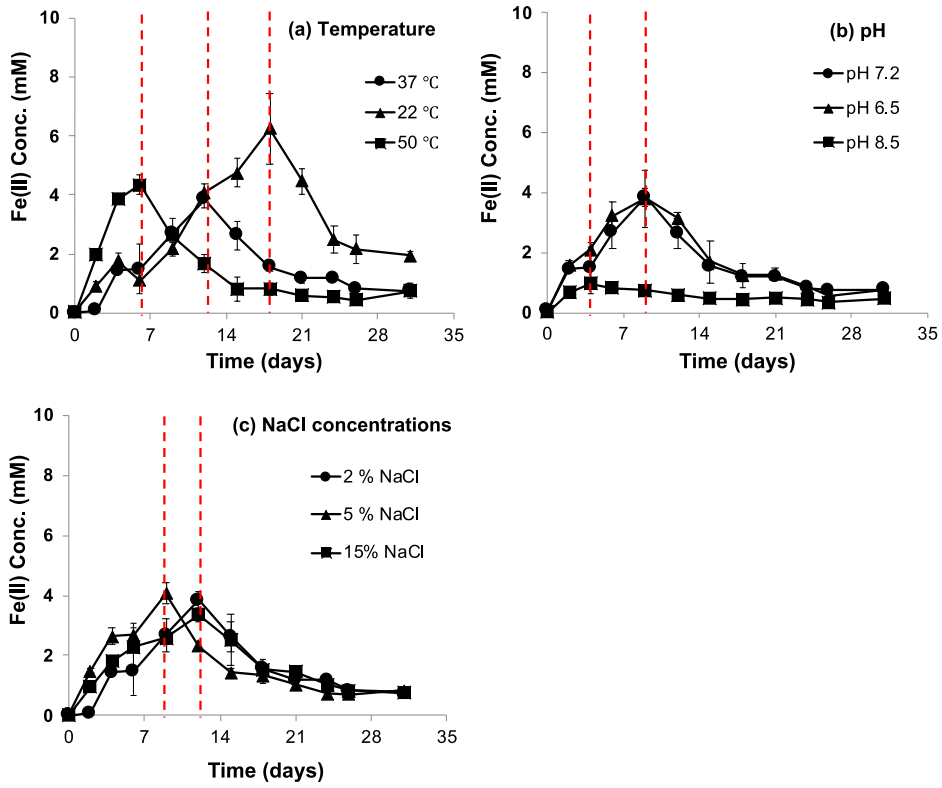

Figure S1. Changes in dissolved Fe(II) over time for the cultures incubated at different temperatures (a), pH (b), and NaCl concentrations (c). The plots are the average of triplicate samples and the error bars indicate standard deviations. The red dashed line identifies the inflection points for biogenic Fe(II)(aq) concentrations. For all the samples, the abiotic controls prepared under the same conditions did not show changes in biogenic Fe(II) concentrations and thus were not included.

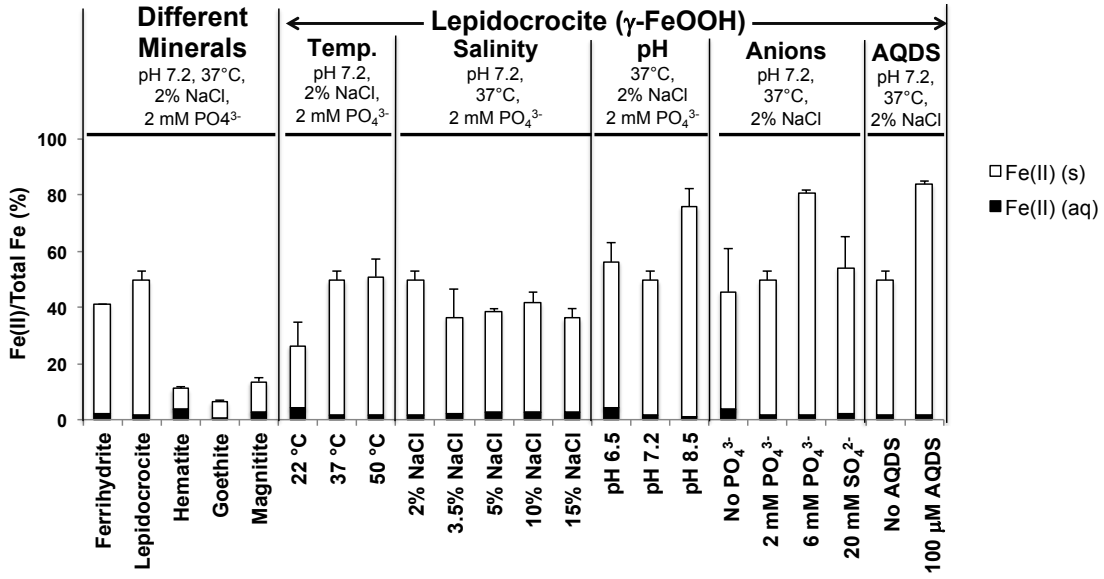

Figure S2. Extractable Fe(II) content (0.5 M HCl for 1 hr) at the end of the experiments, as percentage of total Fe in the reactor. Each bar is further divided into dissolved Fe(II) fraction (filled area) and solid-associated Fe(II) fraction (open area) for the different culturing conditions. Error bars indicate the standard deviation from three replicates.

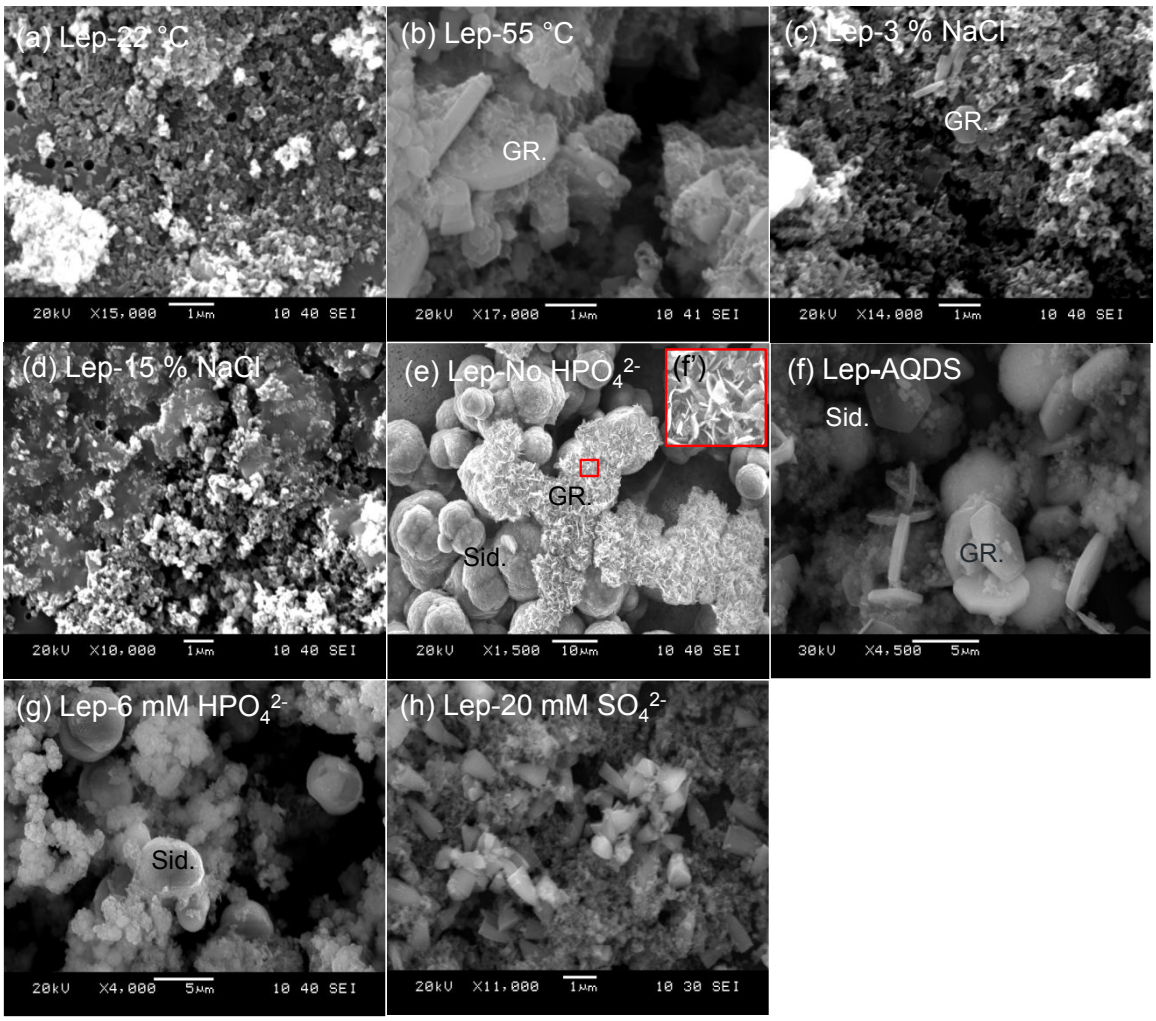

Figure S3. SEM images of the secondary mineral morphology in representative lepidocrocite-reducing cultures (Conditions 1-3, 6, and 9-12 in Table S1). The biominerals that were determined based on previously reported morphologies are labeled as indicated. Abbreviations: Sid (siderite), GR (green rust), and Viv (vivianite). The image of the Lep-15% NaCl reactor (d) shows the same mineral morphology as in the images of samples amended with 5 and 10% NaCl, so the latter are not shown. Note the difference in scales in the micrographs.

(a)

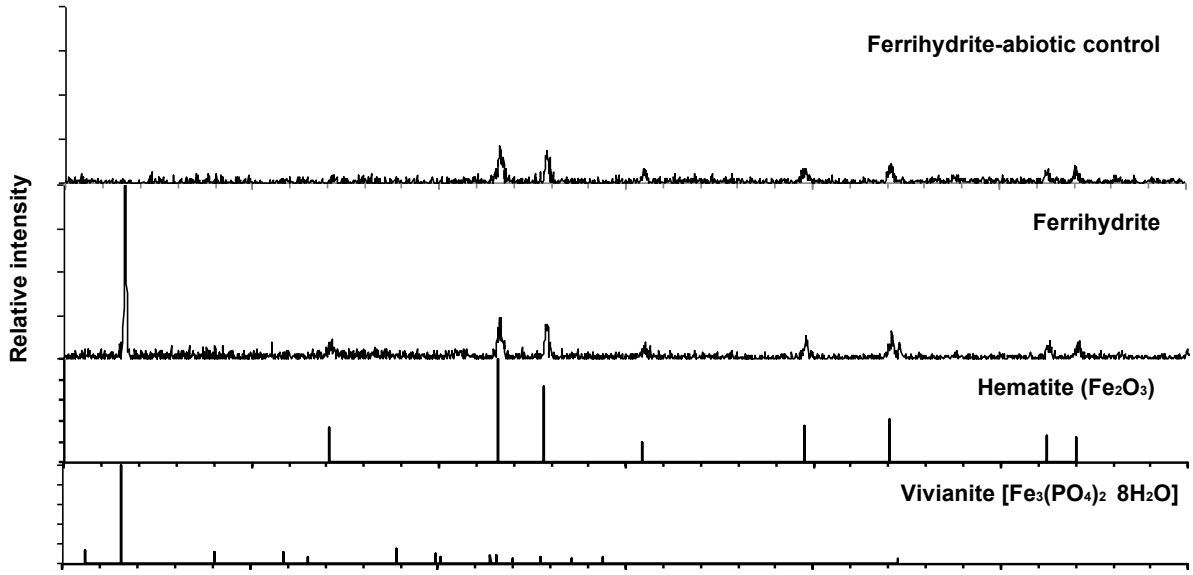
Ferrihydrite-abiotic control
Ferrihydrite
Hematite (Fe_2O_3)
Vivianite [$Fe_3(PO_4)_2$ $8H_2O$]
Relative intensity

(b)

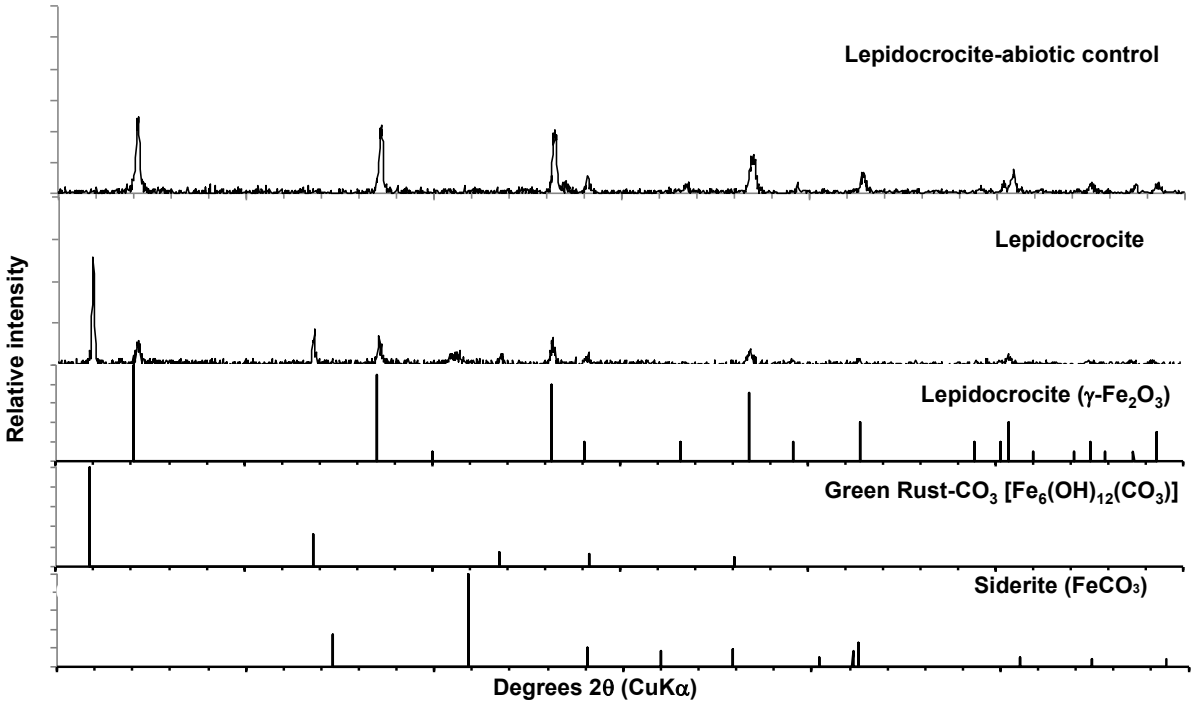
Lepidocrocite-abiotic control
Lepidocrocite
Lepidocrocite (γ-Fe_2O_3)
Green Rust-CO_3 [$Fe_6(OH)_{12}(CO_3)$]
Siderite ($FeCO_3$)
Relative intensity
Degrees 2θ (CuKα)

(c)

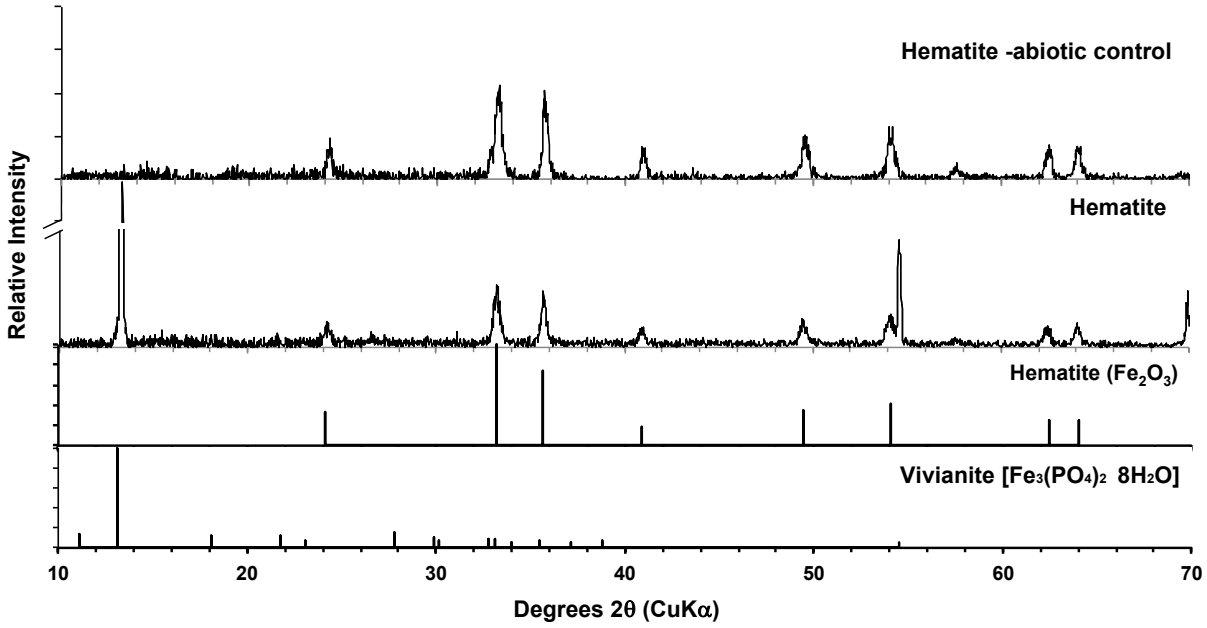
Hematite -abiotic control
Hematite
Hematite (Fe_2O_3)
Vivianite [$Fe_3(PO_4)_2$ $8H_2O$]
Relative Intensity
10
20
30
40
50
60
70
Degrees 2θ (CuKα)

(d)

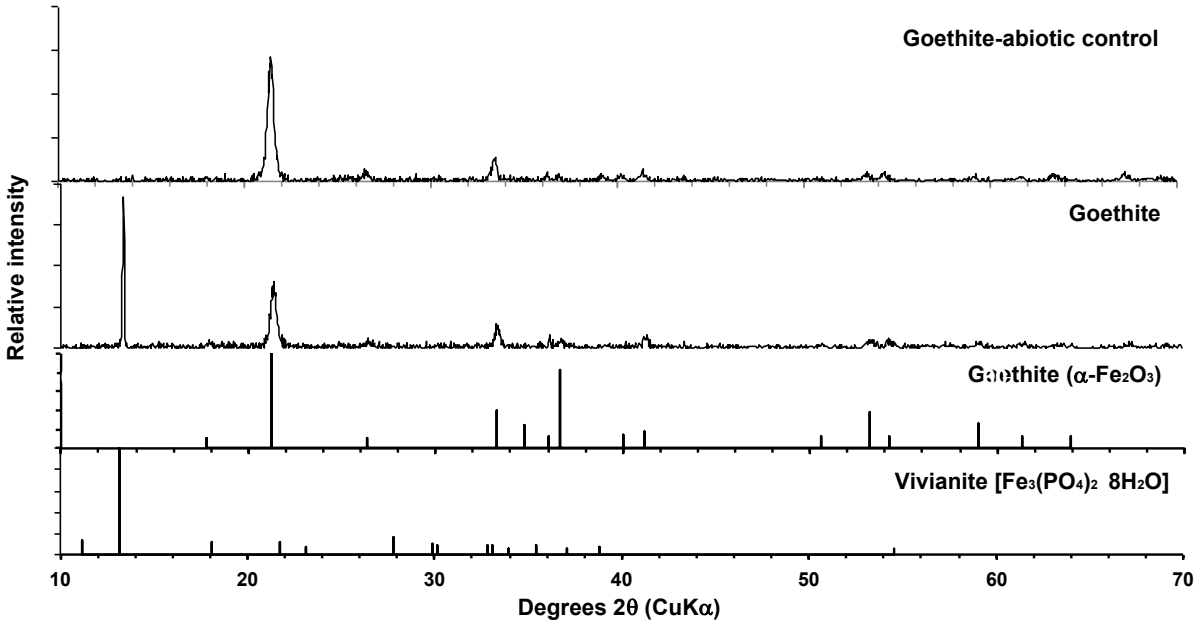
Goethite-abiotic control
Goethite
Goethite (α-Fe_2O_3)
Vivianite [$Fe_3(PO_4)_2$ $8H_2O$]
Relative intensity
10
20
30
40
50
60
70
Degrees 2θ (CuKα)

(e)

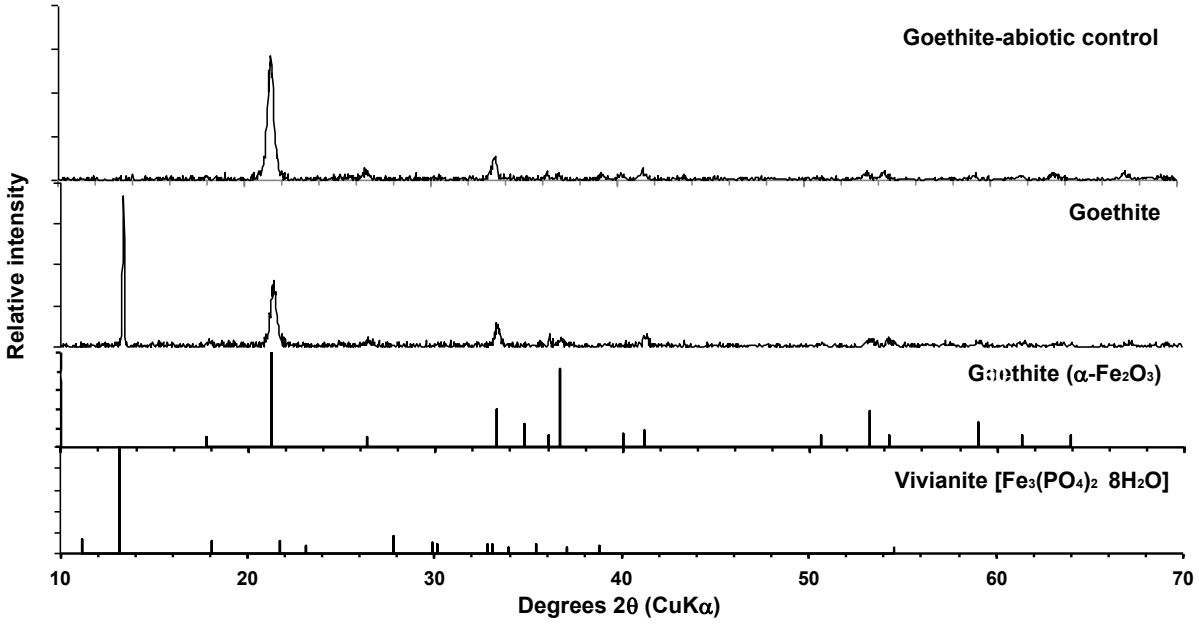

Figure S4. XRD patterns of the solids in cultures incubated under identical conditions but amended with different minerals: ferrihydrite (a), lepidocrocite (b), hematite (c), goethite (d) and magnetite (e) (Conditions 13-17 in Table S1). The cultures were prepared with 2% NaCl at pH 7.2 and incubated at 37 °C. The corresponding abiotic controls were prepared and incubated under the same conditions as the active reactors, except for without inoculation.

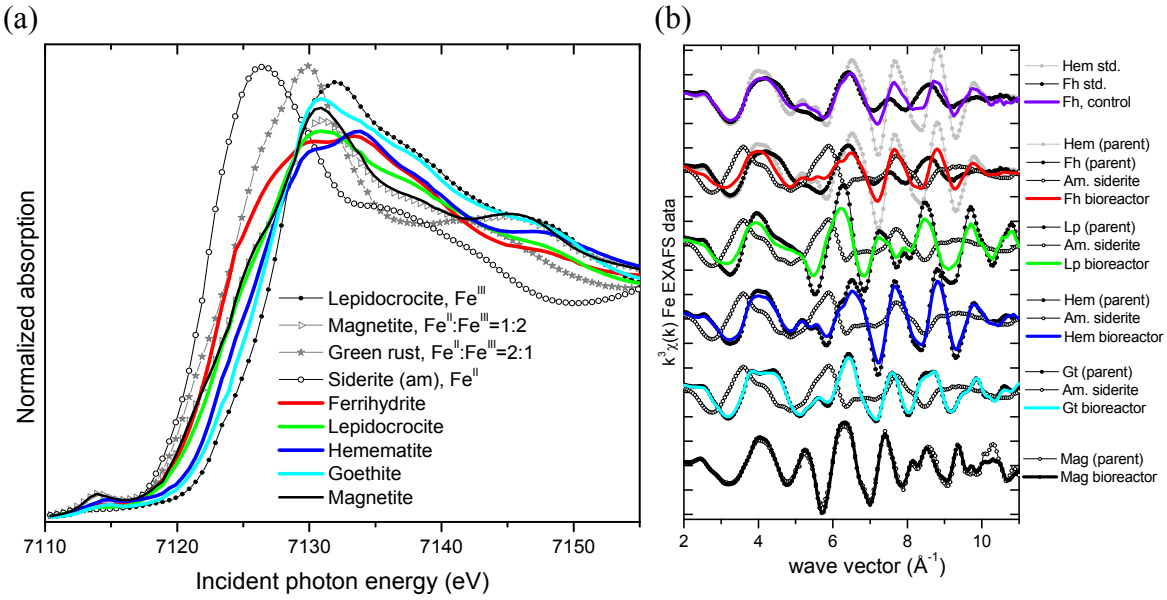

Figure S5. Comparisons of the Fe K-edge XANES (a) and EXAFS (b) spectra from the bioreactors created under the same solution conditions but with different starting Fe minerals (lines) to Fe standards (symbols) (Conditions 13-17 in Table S1). In general, a shift of the edge energy position to lower energy indicates a greater proportion of reduced Fe(II). Panel (b) compares the EXAFS spectra of the bioreactors to the main endmember species determined by the LC analysis, illustrating the intermediate positions of the spectra relative to the standards, as well as several isosbestic points. Panel b-top also shows the spectrum from the uninoculated ferrihydrite control, the intermediate position between the ferrihydrite and the hematite spectra indicates partial abiotic transformation of ferrihydrite to hematite. Abbreviations: Hem: hematite; Fh: ferrihydrite; Am. siderite: amorphous siderite; Mag: magnetite; Gt: goethite.

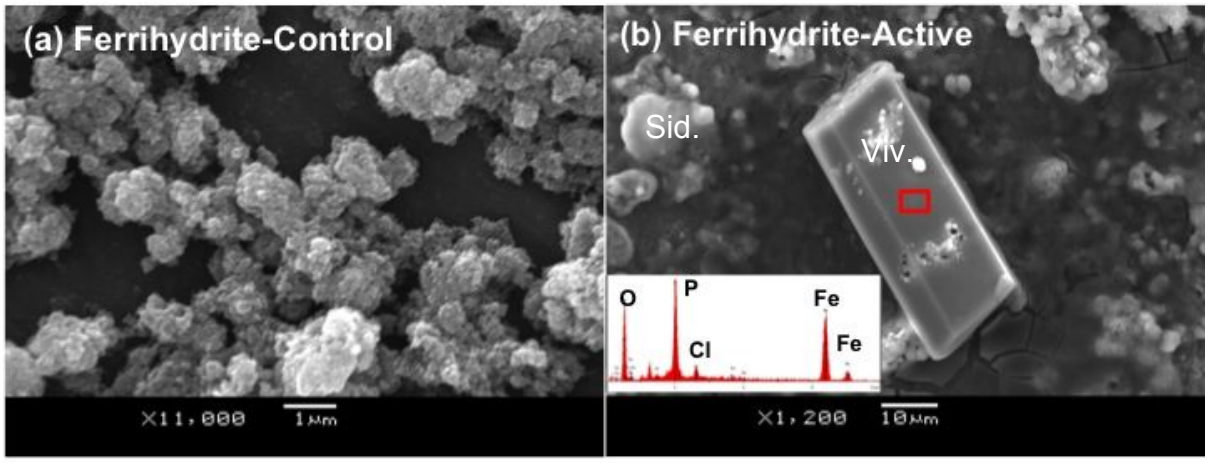

Figure S6. SEM-EDX images of the solids in the ferrihydrite-containing cultures in the absence (a) and in the presence (b) of strain Z6 (note the difference in scale). The prismatic morphology illustrated in (b) is consistent with vivianite identified using XRD. The EDX spectrum of the framed area is shown in the inset. Abbreviations: Sid.: siderite; Viv.: vivianite.

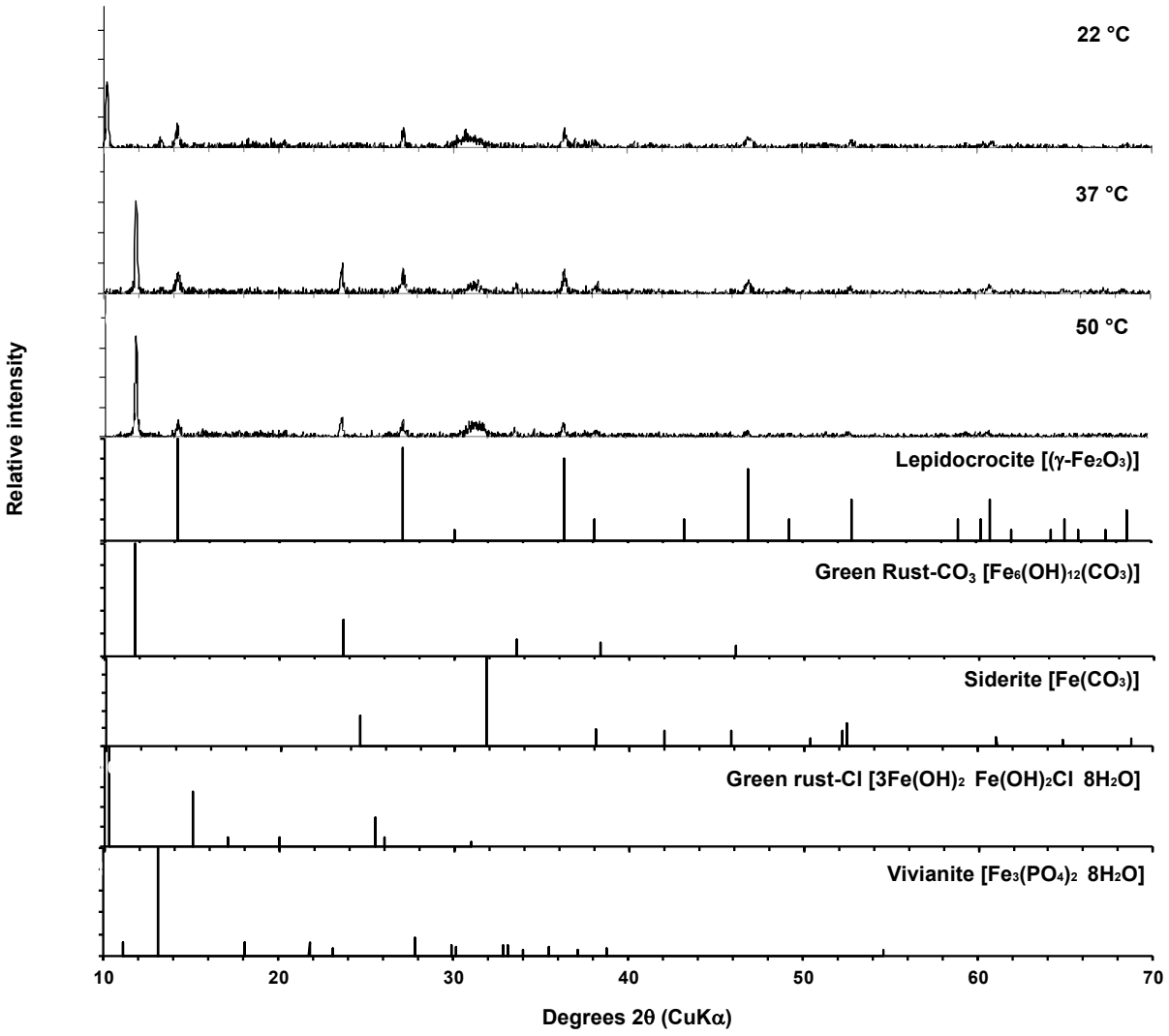

Figure S7. XRD patterns of solids in the lepidocrocite-reducing cultures under different temperatures (Conditions 1, 2 and 14 in Table S1). The cultures were prepared with 2% NaCl, 2 mM phosphate, and buffered at pH 7.2.

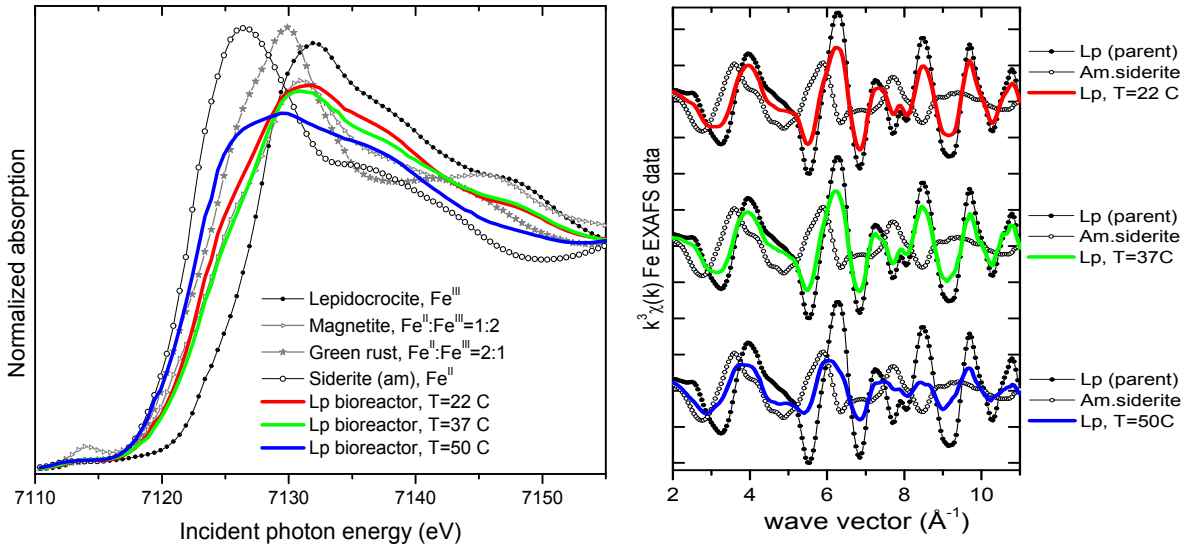

Figure S8. Comparisons of the Fe K-edge XANES (a) and EXAFS spectra (b) from the lepidocrocite bioreactors at different temperatures (lines) to Fe standards (symbols) (Conditions 1, 2 and 14 in Table S1). In general, a shift of the edge energy position to lower energy indicates a greater proportion of reduced Fe(II). Panel (b) compares the EXAFS spectra of the bioreactors to the main endmember species determined by the LC analysis, illustrating the intermediate positions of the spectra relative to the standards, as well as several isosbestic points. Abbreviations: Lp: lepidocrocite; Am. siderite: amorphous siderite.

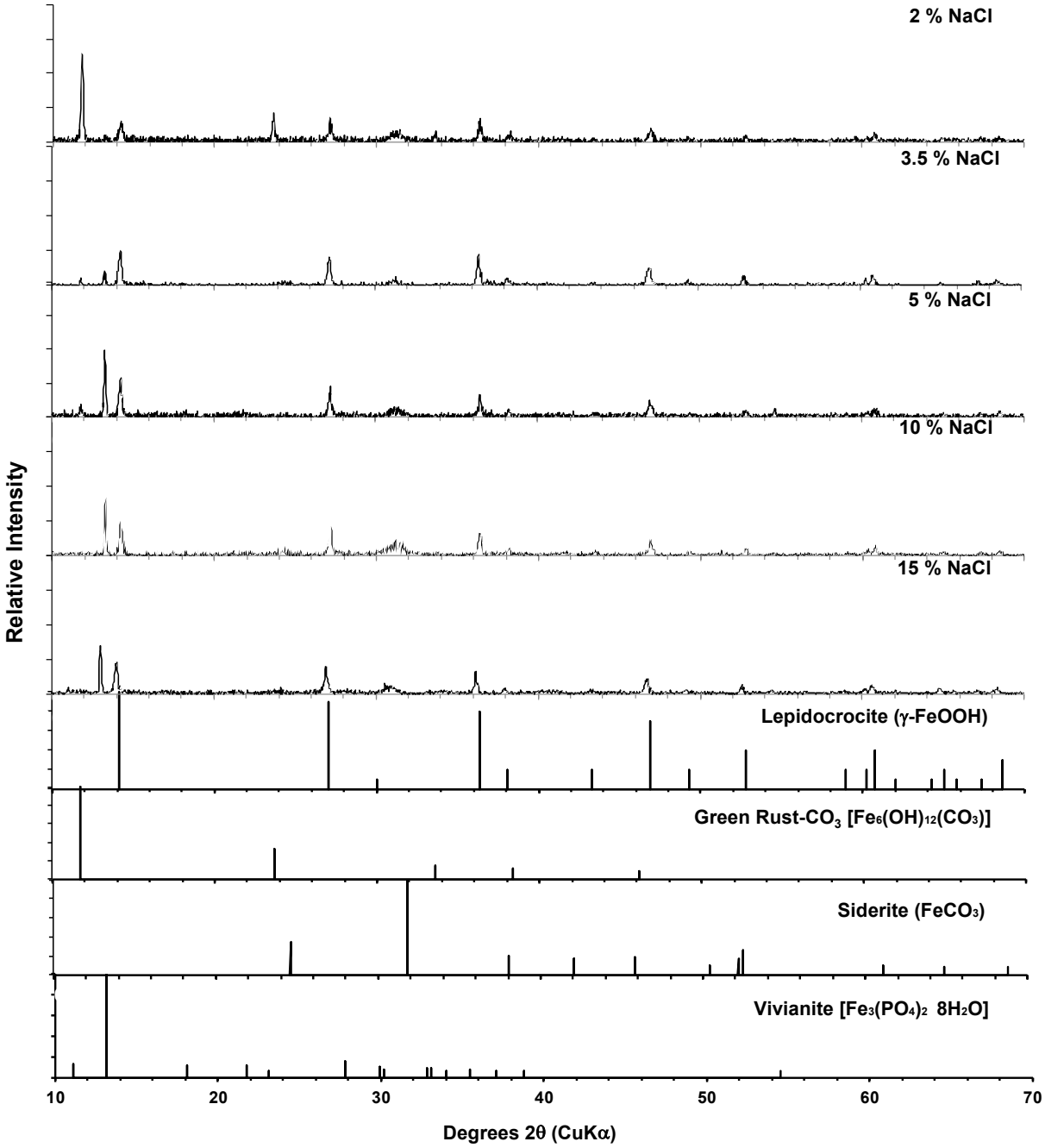

Figure S9. XRD patterns of solids in the lepidocrocite-reducing cultures under different salt concentrations (Conditions 3-6 and 14 in Table S1). The cultures were prepared with 2 mM phosphate at pH 7.2 and incubated at 37 °C.

(a) (b)

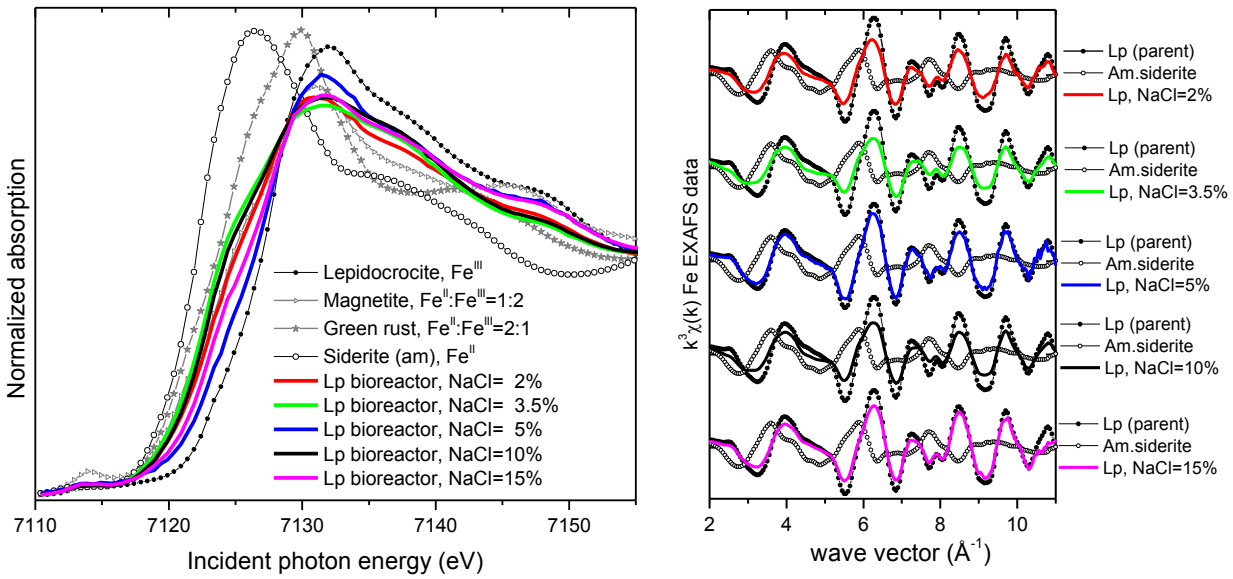

Figure S10. Comparisons of the Fe K-edge XANES (a) and EXAFS spectra (b) from the lepidocrocite (Lp) bioreactors at different NaCl concentrations (lines) to Fe standards (symbols). (Conditions 3-6 and 14 in Table S1). In general, a shift of the edge energy position to lower energy indicates a greater proportion of reduced Fe(II). Panel (b) compares the EXAFS spectra of the bioreactors to the main endmember species determined by the LC analysis, illustrating the intermediate positions of the spectra relative to the standards, as well as several isosbestic points. Abbreviations: Lp: lepidocrocite; Am. siderite: amorphous siderite.

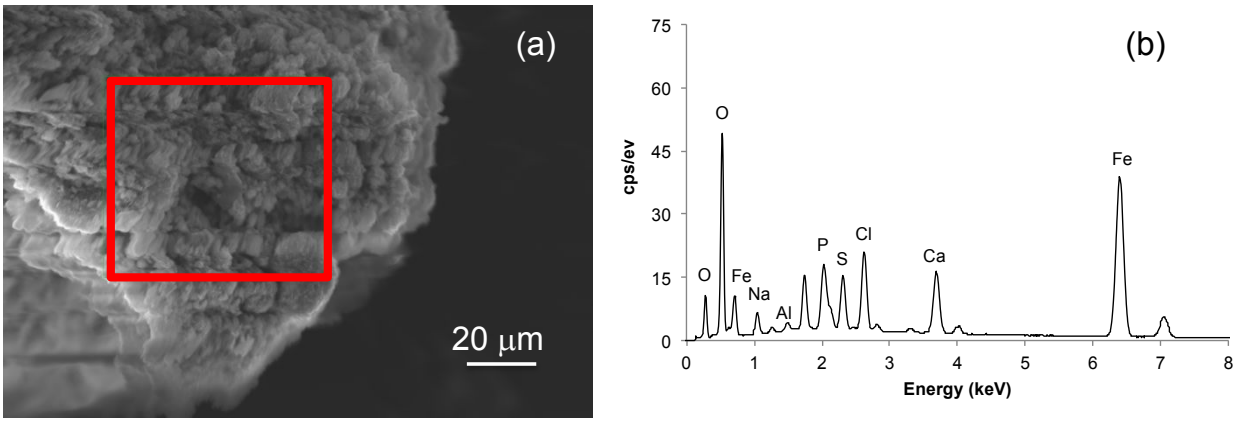

Figure S11. SEM-EDS analyses of the secondary minerals formed in Lep-pH 8.5 (Condition 8 in Table S1). The region in the red frame in (a) was analyzed for element composition as illustrated in (b).

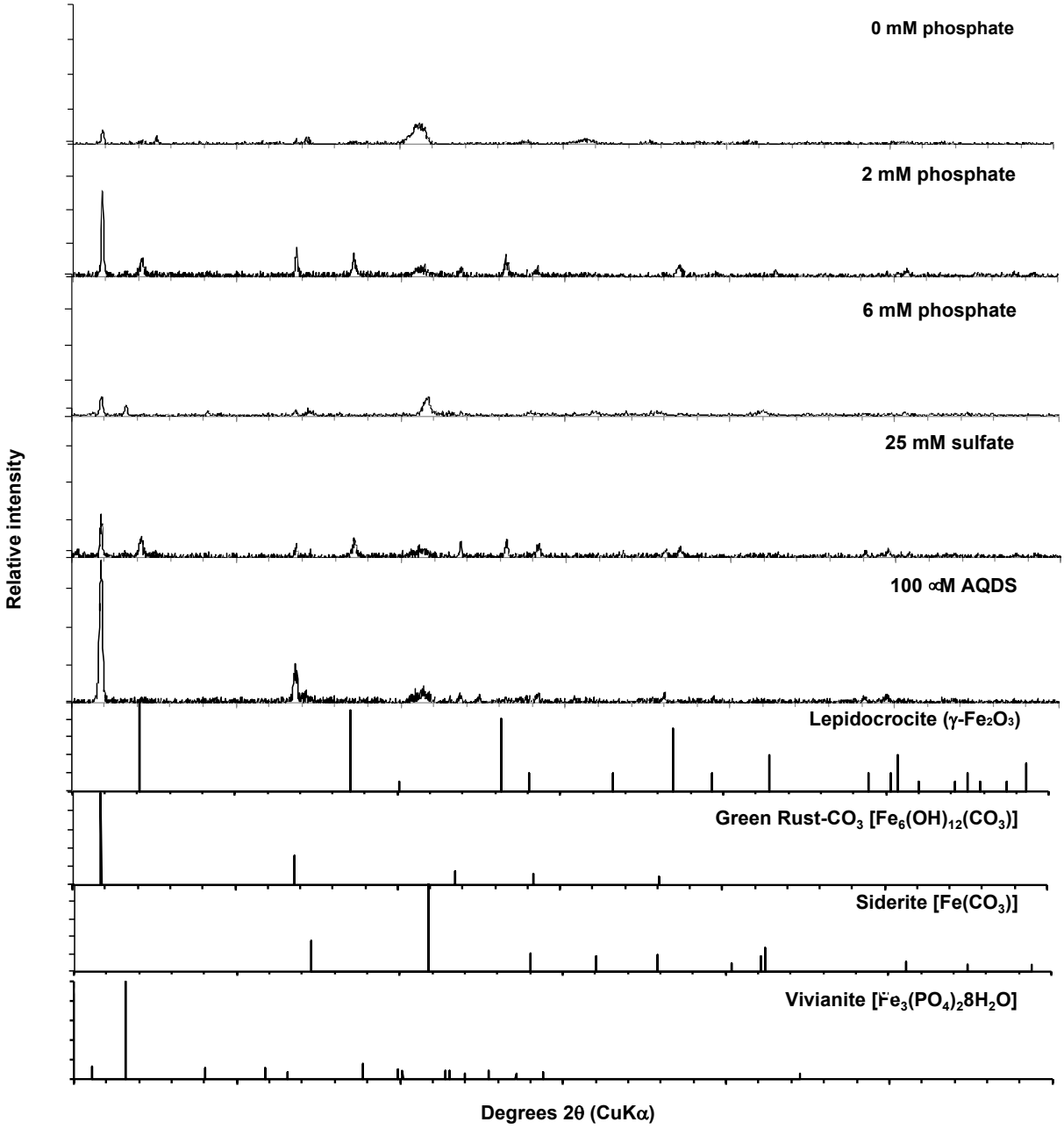

Figure S12. XRD patterns of solids in the lepidocrocite-reducing cultures amended with different anions (Conditions 9-12 and 14 in Table S1). The cultures were prepared with at 2% NaCl, at pH 7.2 and incubated at 37 °C.

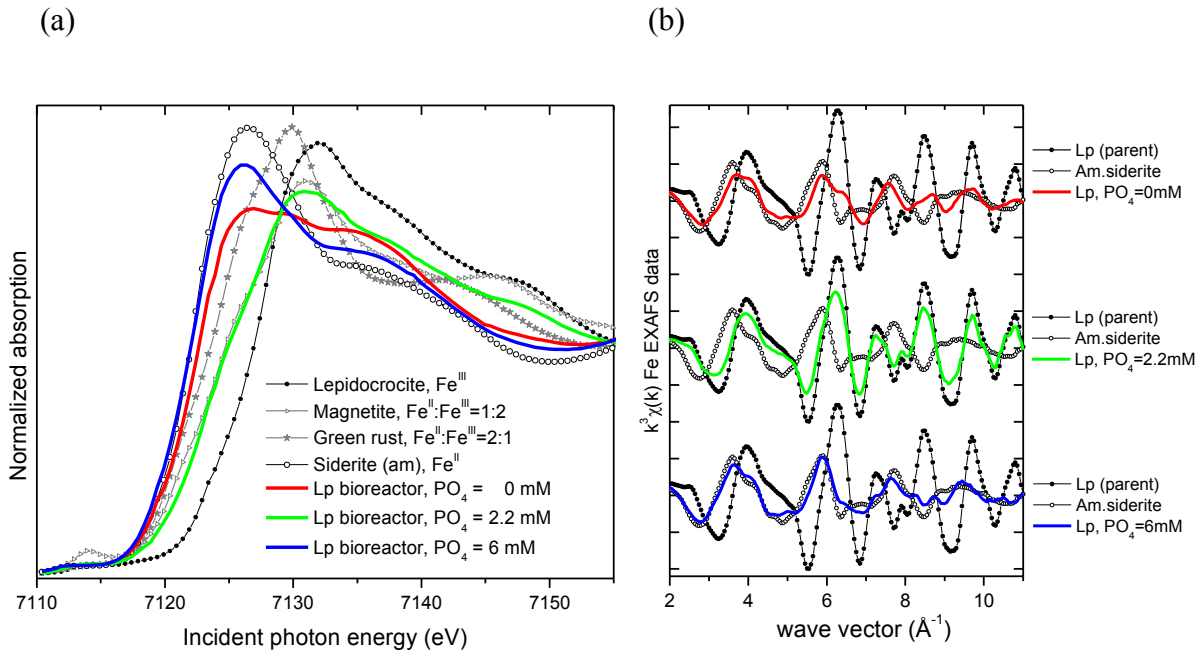

Figure S13. Comparisons of the Fe K-edge XANES (a) and EXAFS (b) spectra from the lepidocrocite (Lp) bioreactors at different phosphate concentrations (lines) to Fe standards (symbols) (Conditions 9-10 and 14 in Table S1). In general, a shift of the edge energy position to lower energy indicates a greater proportion of reduced Fe(II). Panel (b) compares the EXAFS spectra of the bioreactors to the main endmember species determined by the LC analysis, illustrating the intermediate positions of the spectra relative to the standards, as well as several isosbestic points. Abbreviations: Lp: lepidocrocite; Am. siderite: amorphous siderite.

(a) (b)

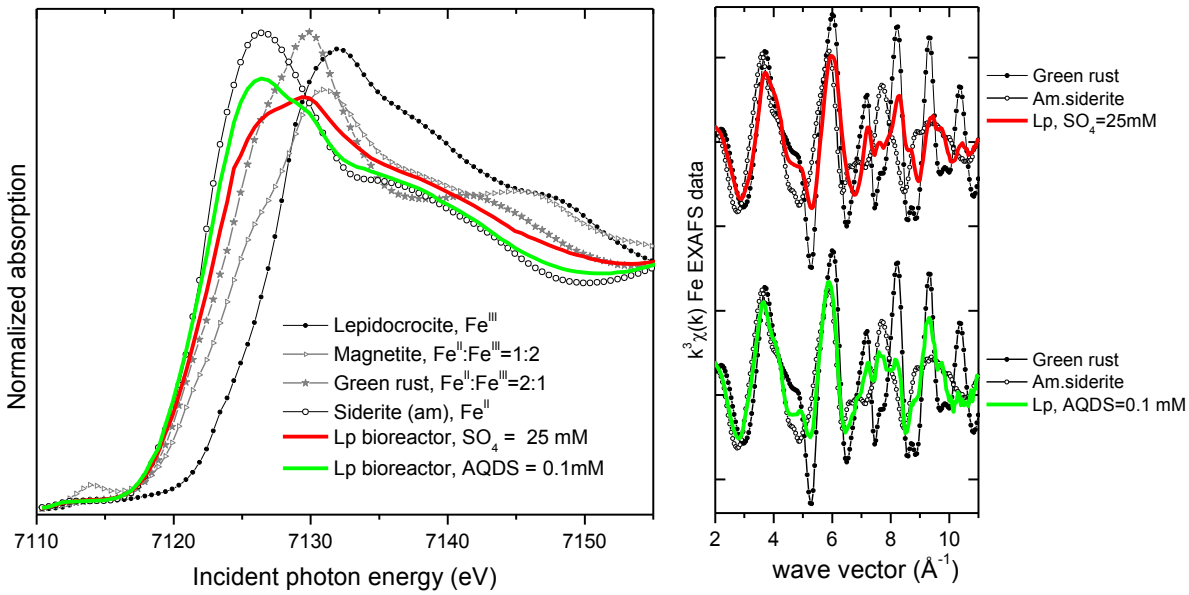

Figure S14. Comparisons of the Fe K-edge XANES (a) and EXAFS (b) spectra from the lepidocrocite bioreactors with amended sulfate or AQDS (lines) to Fe standards (symbols). (Conditions 11 and 12 in Table S1). In general, a shift of the edge energy position to lower energy indicates a greater proportion of reduced Fe(II). Panel (b) compares the EXAFS spectra of the bioreactors to the main endmember species determined by the LC analysis, illustrating the intermediate positions of the spectra relative to the standards, as well as several isosbestic points.

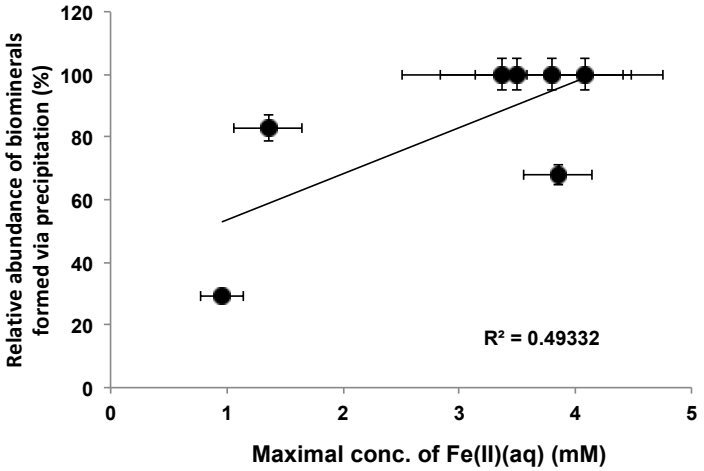

Figure S15. No clear relation is indicated between maximal concentrations of Fe(II)(aq) and the composition of ferrous biominerals. The relative abundance of secondary minerals was based on the XAFS/XANES analyses and minerals presumably formed via precipitation (e.g., siderite and vivianite) (Table 1). The x-axis error bars indicate the standard deviation of triplicate samples and the y-axis error bars signify the maximal uncertainties of the XAFS/XANES analyses

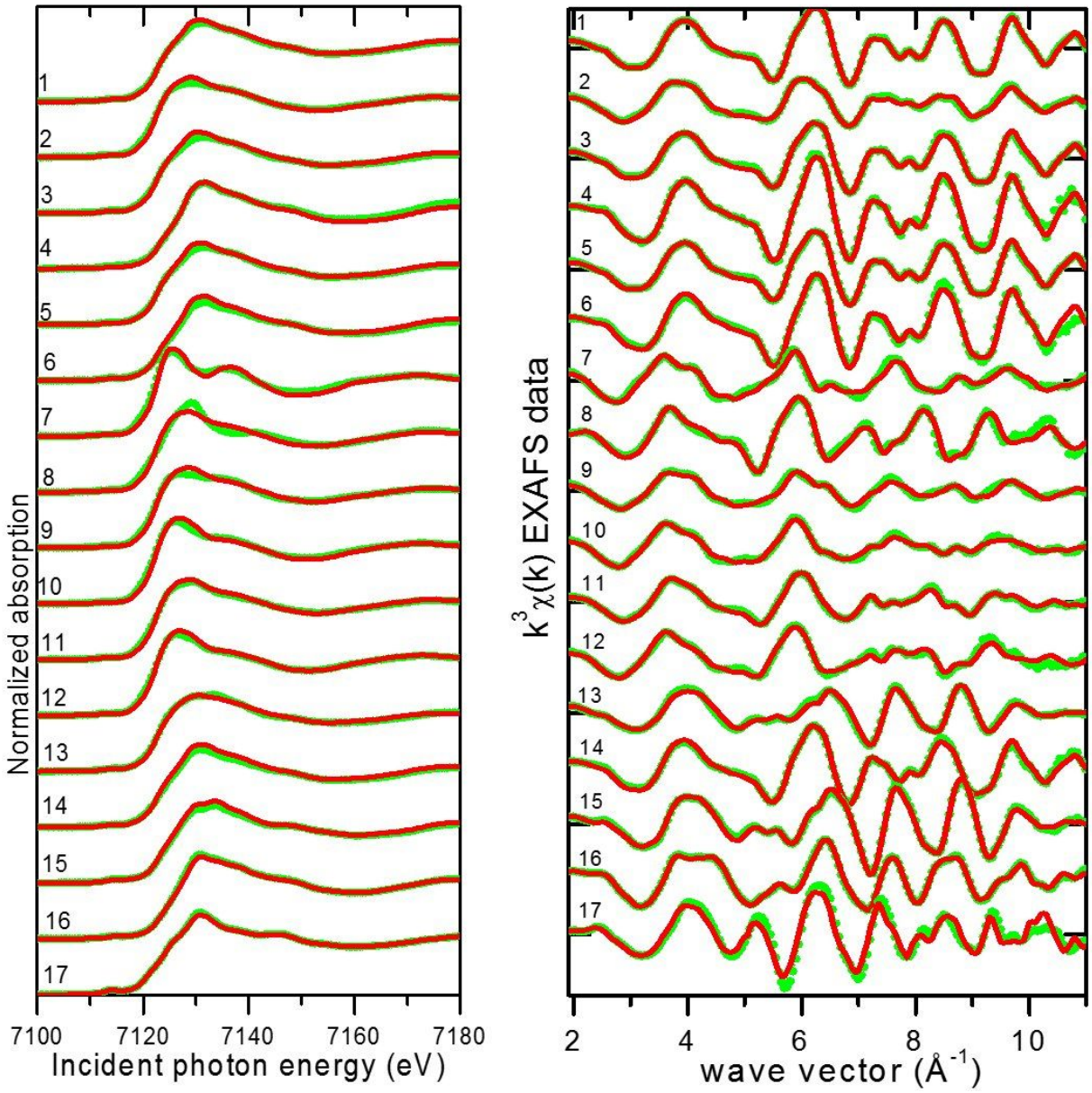

Figure S16. Illustration of the fit quality in the linear combination (LC) analysis of the XANES and EXAFS data. The numbers next to the spectra correspond to the reactor conditions in Table S1. The proportions of each end-member spectrum fit to the experimental data are listed in Table S3.

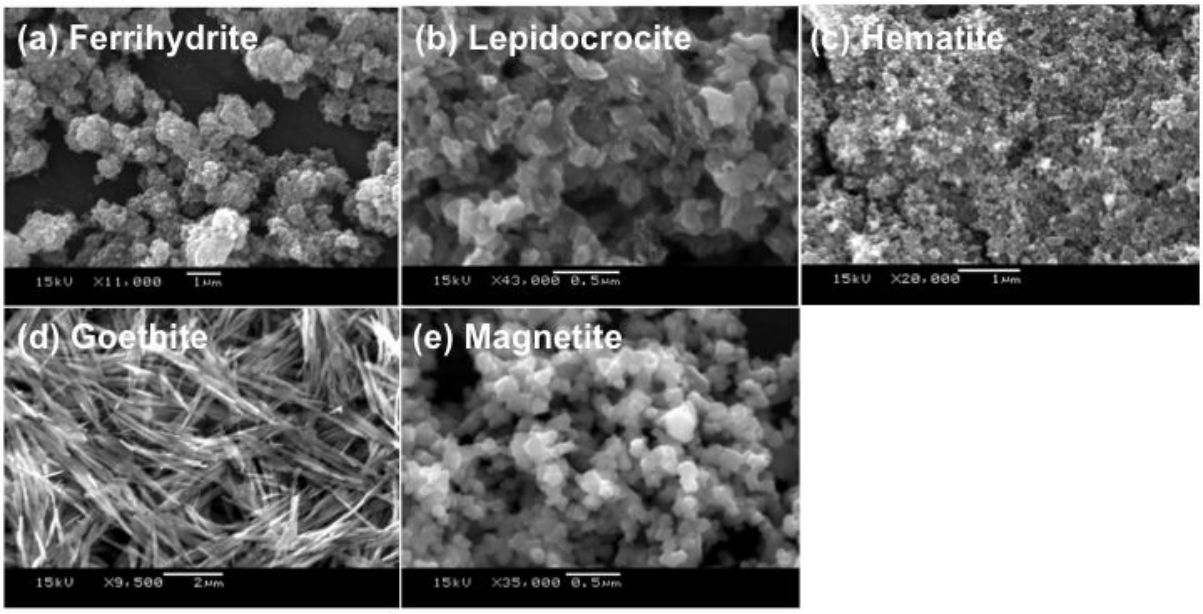

Figure S17. SEM images of the synthesized ferric iron minerals used in this study. Note: the scale bars are different in individual micrographs. No changed in the morphology was observed in the abiotic (sterile) controls.

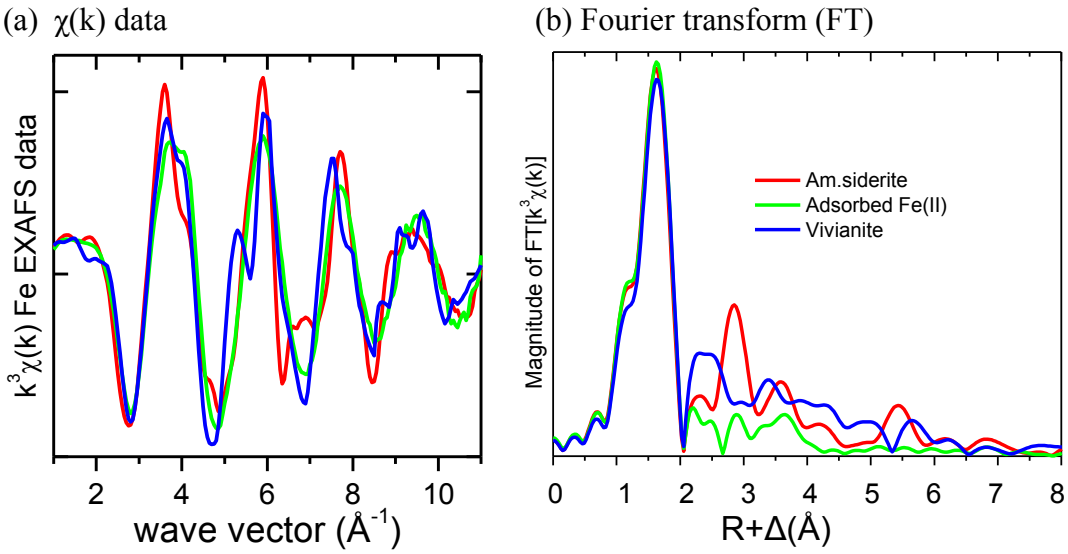

Figure S18. Comparisons of the Fe K-edge EXAFS spectra from adsorbed Fe(II), amorphous siderite, and vivianite. The spectra are nearly identical in their main frequency, amplitude, and phase (reflected in the identical main peak in the FT, i.e., the O-shell coordination environment), and differ only in the outer-shell region, which is of smaller amplitude. The similarity in the main features limits our ability to discern between these Fe(II) phases when their relative spectral content becomes small (e.g., 10-20% of the spectral signal).

(a) 0.5N HCl extraction (b) XANES

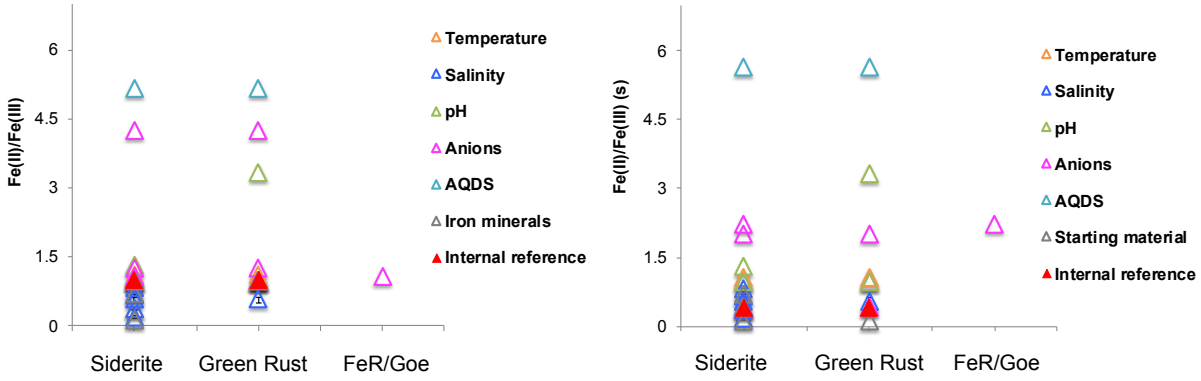

Figure S19. Fe(II)/Fe(III) calculated using the Fe(II) concentrations determined by 0.5 N HCl extraction (a) and XANES (b) for the conditions with siderite, green rust and FeR/Goe. The results showed similar trends between the two Fe(II) quantification methods in that formation of specific secondary mineral could not be explained by the ratios of Fe(II)/Fe(III). Only siderite, green rust and ferrihydrite (Fh)/goethite (Goe) as the major secondary minerals (≥10%) determined by XANES and EXAFS were considered. The subfigure (a) is the same as Fig. 2c in the main text of manuscript. In (b), the condition Lep_pH 6.5 was not included because nearly 100 % of the solid phase was Fe(II) and the calculated Fe(II)/Fe(III) value was infinite. The internal reference indicated the cultures prepared with lepidocrocite, 2% NaCl, pH 7.2, 2.5 mM phosphate, no sulfate and at 37 °C.

References

1. Dworkin, M.; Falkow, S.; Rosenberg, E.; Schleifer, K. H.; Stackebrandt, E., Bacteria: Firmicutes, Cyanobacteria. In *The Prokaryotes: A Handbook on the Biology of Bacteria*, Springer Science&Business Media, LLC: New York, 2006.

2. Dong, Y.; Sanford, R. A.; Boyanov, M. I.; Kemner, K. M.; Flynn, T. M.; O'Loughlin, E. J.; Chang, Y. J.; Locke, R. A.; Weber, J. R.; Egan, S. M.; Mackie, R. I.; Cann, I.; Fouke, B. W., *Orenia metallireducens* sp. nov. strain Z6, a novel metal-reducing Firmicute from the deep subsurface. *Appl. Environ. Microbiol.* **2016,** *82*(21), 6440-6453.

3. Dong, Y.; Sanford, R. A.; Chang, Y. J.; McInerney, M. J.; Fouke, B. W., Hematite reduction buffers acid generation and enhances nutrient uptake by a fermentative iron reducing bacterium, *Orenia metallireducens* Strain Z6. *Environ. Sci. Technol.* **2017,** *51*(1), 232-242.

4. Schwertmann, U.; Cornell, R. M., *Iron Oxides in the Laboratory: Preparation and Characterization*. 2nd ed.; Wiley-VCH Verlag GmbH: Weinheim, 2000; p 188.

5. Fredrickson, J. K.; Zachara, J. M.; Kennedy, D. W.; Dong, H.; Onstott, T. C.; Hinman, N. W.; Li, S. M., Biogenic iron mineralization accompanying the dissimilatory reduction of hydrous ferric oxide by a groundwater bacterium. *Geochim. Cosmochim. Acta* **1998,** *62*, 3239-3257.

6. Gibbs, C. R., Characterization and application of ferrozine iron reagent as a ferrous iron indicator. *Anal. Chem.* **1976,** *48*(8), 1197-1200.

7. Stookey, L. L., Ferrozine - a new spectrophotometric reagent for iron. *Anal. Chem.* **1970,** *42*(7), 779.

8. Lovley, D. R.; Phillips, E. J., Rapid assay for microbially reducible ferric iron in aquatic sediments. *Appl. Environ. Microbiol.* **1987,** *53*(7), 1536-1540.

9. Dong, Y.; Sanford, R. A.; Locke, R. A.; Cann, I. K.; Mackie, R. I.; Fouke, B. W., Fe-oxide grain coatings support bacterial Fe-reducing metabolisms in 1.7-2.0 km-deep subsurface quartz arenite sandstone reservoirs of the Illinois Basin (USA). *Front. Microbiol.* **2014,** *5*, 511.

10. O'Loughlin, E. J.; Gorski, C. A.; Scherer, M. M.; Boyanov, M. I.; Kemner, K. M., Effects of oxyanions, natural organic matter, and bacterial cell numbers on the bioreduction of lepidocrocite (gamma-FeOOH) and the formation of secondary mineralization products. *Environ. Sci. Technol.* **2010,** *44*(12), 4570-4576.

11. Kemner, K. M.; Kelly, S. D., Synchrotron-based Techniques for Monitoring Metal Tranformations. In *Manual of Environmental Microbiology*, Hurst, C. J., Ed. ASM Press: Washington DC, 2007; pp 1183-1194.

12. Kropf, A. J.; Katsoudas, J.; Chattopadhyay, S.; Shibata, T.; Lang, E. A.; Zyryanov, V. N.; Ravel, B.; Mclvor, K.; Kemner, K. M.; Scheckel, K. G.; Bare, S. R.; Terry, J.; Kelley, S. D.; Bunker, B. A.; Segre, C. U., The new MRCAT (Sector 10) bending magnet beamline at the Advanced Photon Source. In *AIP Conference Proceedings*, Garrett, R.; Gentle, I.; Nugent, K.; Wilkins, S., Eds. 2010; pp 299-302.

13. O'Loughlin, E. J.; Kelly, S. D.; Cook, R. E.; Csencsits, R.; Kemner, K. M., Reduction of Uranium(VI) by mixed iron(II/iron(III) hydroxide (green rust): Formation of UO2 nanoparticles. *Environ. Sci. Technol.* **2003,** *37*(4), 721-727.

14. Dong, Y. R.; Sanford, R. A.; Boyanov, M. I.; Kemner, K. M.; Flynn, T. M.; O'Loughlin, E. J.; Chang, Y. J.; Locke, R. A.; Weber, J. R.; Egan, S. M.; Mackie, R. I.; Cann, I.; Fouke, B. W., *Orenia metallireducen*s sp nov Strain Z6, a Novel Metal- Reducing Member of the Phylum Firmicutes from the Deep Subsurface. *Appl. Environ. Microbiol.* **2016,** *82*(21), 6440-6453.

15. Kwon, M. J.; O'Loughlin, E. J.; Boyanov, M. I.; Brulc, J. M.; Johnston, E. R.; Kemner, K. M.; Antonopoulos, D. A., Impact of Organic Carbon Electron Donors on Microbial Community Development under Iron- and Sulfate-Reducing Conditions. *Plos One* **2016,** *11*(1).

16. Kwon, M. J.; Yang, J. S.; Shim, M. J.; Boyanov, M. I.; Kemner, K. M.; O'Loughlin, E. J., Acid Extraction Overestimates the Total Fe(II) in the Presence of Iron (Hydr)oxide and Sulfide Minerals. *Environ. Sci. Technol. Lett.* **2014,** *1*(7), 310-314.

17. Kwon, M. J.; Boyanov, M. I.; Antonopoulos, D. A.; Brulc, J. M.; Johnston, E. R.; Skinner, K. A.; Kemner, K. M.; O'Loughlin, E. J., Effects of dissimilatory sulfate reduction on Fe-III (hydr)oxide reduction and microbial community development. *Geochim. Cosmochim. Acta* **2014,** *129*, 177-190.

18. O'Loughlin, E. J.; Boyanov, M. I.; Flynn, T. M.; Gorski, C. A.; Hofmann, S. M.; McCormick, M. L.; Scherer, M. M.; Kemner, K. M., Effects of Bound Phosphate on the Bioreduction of Lepidocrocite (gamma-FeOOH) and Maghemite (gamma-Fe2O3) and Formation of Secondary Minerals. *Environ. Sci. Technol.* **2013,** *47*(16), 9157-9166.

19. Boyanov, M. I.; O'Loughlin, E. J.; Roden, E. E.; Fein, J. B.; Kemner, K. M., Adsorption of Fe(II) and U(VI) to carboxyl-functionalized microspheres: The influence of speciation on uranyl reduction studied by titration and XAFS. *Geochim. Cosmochim. Acta* **2007,** *71*(8), 1898-1912.

20. Newville, M.; Livins, P.; Yacoby, Y.; Rehr, J. J.; Stern, E. A., Near-edge x-ray absorption fine structure of Pb – a comparison of theory and experiment. *Physical Review B* **1993,** *47*(21), 14126-14131.

21. Ravel, B.; Newville, M., ATHENA, ARTEMIS, HEPHAESTUS: data analysis for X-ray absorption spectroscopy using IFEFFIT. *J. Synchrotron Radiat.* **2005,** *12*, 537-541.